ACS Energy Letters

Cite This: ACS Energy Lett. 2019, 4, 2069−2074

http://pubs.acs.org/journal/aelccp

LETTER

Rational Design for Optimizing Hybrid Thermo-triboelectric Generators Targeting Human Activities

Byungseok Seo,[†,§] Youngsun Cha,[†,§] Sangtae Kim,[*,‡] and Wonjoon Choi[*,†]

[†]School of Mechanical Engineering, Korea University, Seoul, 02841, Republic of Korea

[‡]Center for Electronic Materials, Korea Institute of Science and Technology, Seoul, 02792, Republic of Korea

Supporting Information

ABSTRACT: Despite the rise in Internet of Things devices and mobile electronics, devising an energy harvester with sufficient time-averaged power remains a challenge when targeting human activities. Here, we report a hybrid thermo-triboelectric generator targeting human motion with systematic optimization strategies in frequency feature-size variable spaces. The device consists of bismuth telluride (Bi_2Te_3) tiles with polydimethylsiloxane (PDMS) layers filled in between, thereby harvesting both thermal energy and triboelectricity from human touch. Detailed heat transport analyses reveal that optimal operational frequency for thermoelectrics may be tuned on the basis of the insulation property of PDMS. Meanwhile, triboelectricity exhibits strong feature-size dependence when PDMS is interfaced with high-dielectric thermoelectric materials. The analyses establish the design guidelines for a hybrid energy harvester that outperforms the simple physical addition of constituent energy harvesters and demonstrates an average power of 3.27 μW/cm^3, which is feasible to power potential applications operated by human touch at 2.5 Hz.

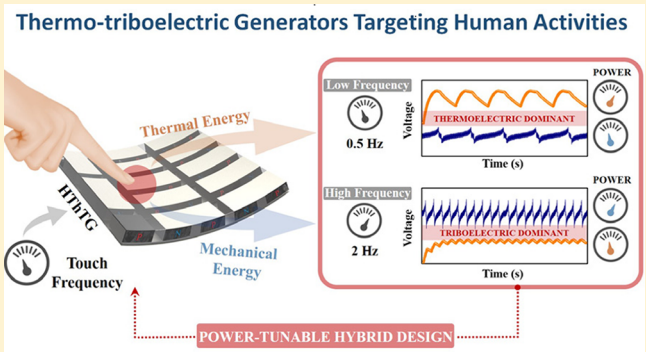

A significant amount of research attention has been paid to harvest human-induced energy into electricity with potential applications in powering wireless sensors or Internet of Things devices.[1,2] Successful integration of energy harvesters into small-scale sensor systems may allow the operation of sensors without battery exchange for years or in remote environments where battery charging is not feasible. Energy harvesters may also provide additional efficiency to the overall electric grid because the amount of generated electricity scales directly with human activity, thereby providing electricity during peak hours and at locations where it is required the most to alleviate the burden on electric grids.

To realize successful energy harvesting, researchers have developed energy harvesters from different sources such as thermal,[3,4] vibrational,[5] acoustic,[6] human-induced,[7,8] or contact electrification-based energies.[9,10] Many of these, however, face severe challenges to commercialization due to the limited efficiency linked to their fundamental working mechanisms. For instance, thermoelectric generators targeting human body heat need to overcome quick thermal saturation that degrades output electricity significantly.[11] Detailed thermal analyses have shown that utilizing more than 50% of fill factor in thermoelectric generators decreases the output power due to thermal saturation.[12] Piezoelectric and triboelectric generators suffer from the mismatch between their natural output frequencies and human motion time scales. The generated electricity from these two types of generators often reaches the current peak width within 50 ms; hence, these generators are limited to a human activity time scale of 0.5−5 Hz.[13,14]

Efforts to overcome some of these limitations have been presented by devising hybrid energy harvesters targeting multiple energy sources simultaneously.[15] For instance, various designs to harvest both thermal and mechanical energies have been demonstrated, thereby utilizing thermoelectric, pyroelectric, piezoelectric, and/or triboelectric nanogenerators.[16−18] However, to design hybrid energy harvesters that outperform the simple addition of their components, one must consider the nature of the targeted human motion. For instance, keyboard typing involves fast finger motion with frequencies above 5 Hz, while handholding guide rails may involve natural frequencies as low as 0.1 Hz. Because different energy harvesters exhibit their own distinct characteristic time scales of output power, designing hybrid energy harvesters must involve meticulous

Received: July 3, 2019
Accepted: July 12, 2019
Published: July 12, 2019

Downloaded via COLUMBIA UNIV on October 21, 2019 at 22:19:31 (UTC).
See https://pubs.acs.org/sharingguidelines for options on how to legitimately share published articles.

 © 2019 American Chemical Society

DOI: 10.1021/acsenergylett.9b01426
ACS Energy Lett. 2019, 4, 2069−2074

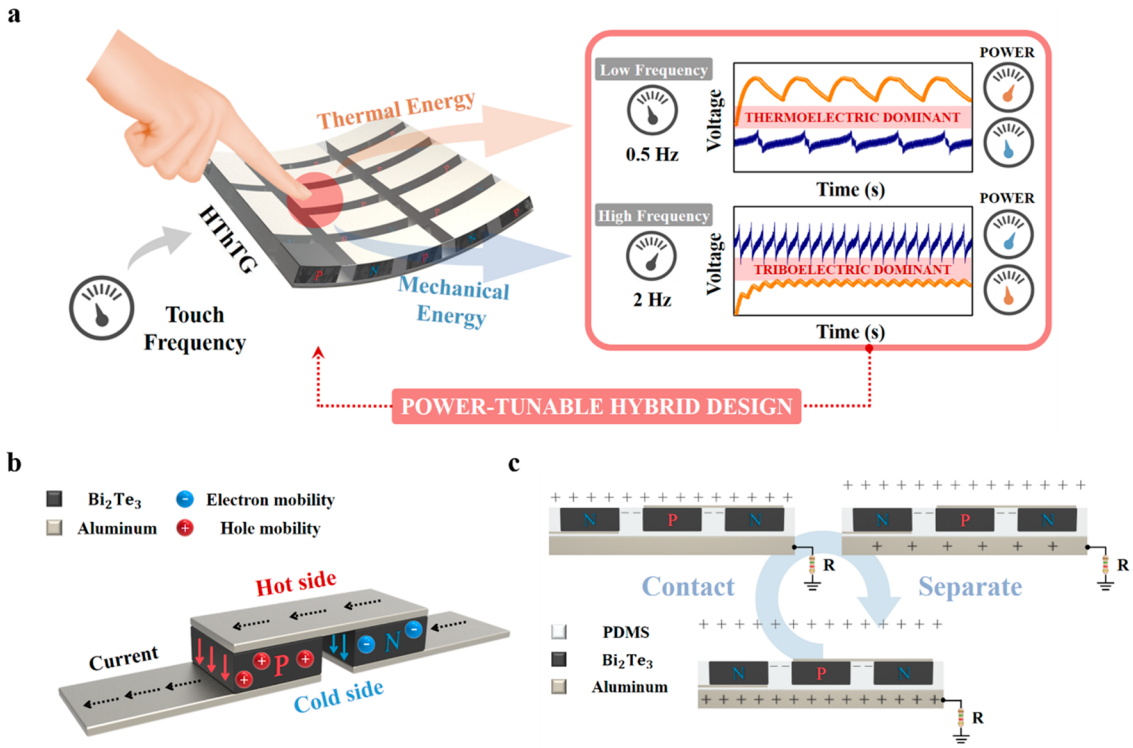

Figure 1. Schematic representation of the working principle of a hybrid thermo-triboelectric generator (HThTG). (a) Device schematic shows p- and n-type Bi_2Te_3 tiles embedded within a polydimethylsiloxane (PDMS) matrix. Finger touch generates electricity from both thermoelectric and triboelectric parts with the relative amounts depending on the touch motion frequency. (b) Thermoelectric power generation through the pn junction upon human touch. (c) Triboelectric power generation via single-electrode mode upon human touch.

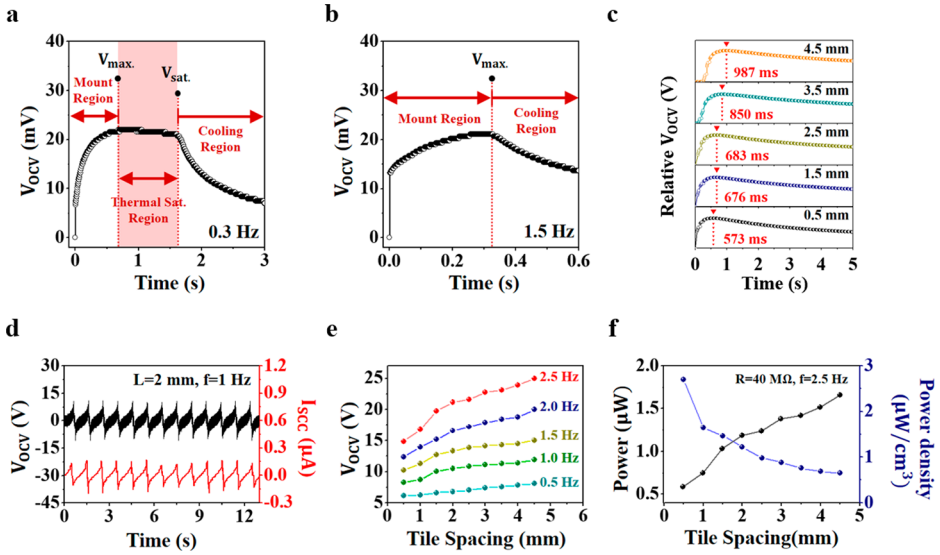

Figure 2. Electrical characteristics and power generation of HThTGs. Open circuit voltage (OCV) generated from the thermoelectric part when human skin (T_h = 35 °C) touches the generator's top surface with (a) 0.3 and (b) 1.5 Hz of input frequency. (c) Temporal voltage evolution when human touch is maintained on HThTG devices with different PDMS widths. (d) OCV and short circuit current (SCC) obtained from triboelectric generators upon human finger touch motion at a frequency of 1 Hz. (e) Triboelectric voltage and (f) generated power and power density based on tile spacing.

optimization of the device physics and careful selection of relevant energy harvesters. Nonetheless, no such optimization has been demonstrated in the literature so far despite the immediate technological relevance of energy harvesters.

Here, we report a hybrid thermo-triboelectric generator (HThTG) targeting human motion with systematic optimization strategies in frequency feature-size variable spaces. The working principle and fabrication process of HThTG are illustrated in Figure 1a and Figure S1, respectively. As one touches the device surface, body heat drives electrons from n-type and holes from p-type bismuth telluride (Bi_2Te_3) to the cold side. By serially connecting p-type and n-type Bi_2Te_3, as shown in Figure 1b, we can harvest electric current from thermoelectric devices. Simultaneously, triboelectric energy is

DOI: 10.1021/acsenergylett.9b01426
ACS Energy Lett. 2019, 4, 2069−2074

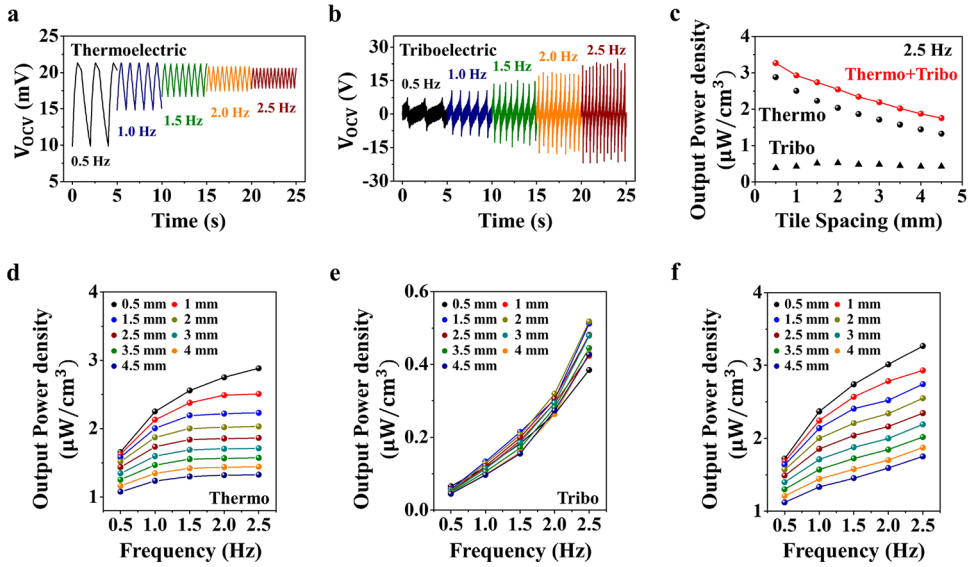

Figure 3. Optimization strategies for HThTG at different input frequencies. (a) Thermoelectric and (b) triboelectric OCV signals for the hybrid generator at different input frequencies. (c) Power density in terms of the total device volume based on tile spacing for the thermoelectric, triboelectric, and hybrid generators. Power density based on input motion frequency for the (d) thermoelectric, (e) triboelectric, and (f) hybrid generators at various tile spacings. The area of contact during touch motion is controlled to be identical in all the cases.

generated when human skin touches the polydimethylsiloxane (PDMS) layers. Due to the large difference in electron affinity between human skin and PDMS, the generated charge polarity at the surface produces potential difference and generates energy (Figure 1c).

The thermoelectric voltage generated by human touch motion exhibits three distinct regions according to the duration and frequency of the heat source. When thermoelectric devices are touched, thermoelectric voltage immediately increases due to temperature difference between the electrodes at both ends (Figure 2a). If the touch is maintained to cause thermal saturation within the Bi_2Te_3 tiles, the increase in voltage stalls and gradually decreases. Upon removal of the heat source, the generated voltage decays quickly as the device cools. We designate these three cases as the mount, saturation, and cooling regions.

Depending on the frequency of input touch, the device may or may not exhibit a saturation region because the heat source may have been quickly removed before thermal saturation occurred. For instance, Figure 2b shows no thermal saturation region when input touch occurs at a frequency of 1.5 Hz as opposed to the clear saturation region observed at 0.3 Hz (Figure 2a). The time interval of the mount region is affected by the thermal resistance surrounding the thermoelectrics, including factors such as PDMS layer thickness, width, and density. Figure 2c shows the voltage response when human touch is maintained for 5 s. The time interval to reach the maximum voltage increases from 573 to 987 ms as the distance between Bi_2Te_3 tiles increases from 0.5 to 4.5 mm. Because thermal saturation is to be avoided, the optimal operational frequency for thermoelectrics must be above ∼1 Hz with the frequency threshold being tunable based on detailed thermal engineering.

The complex thermal behavior within Bi_2Te_3 tiles surrounded by PDMS is analyzed further using finite element analyses. Figure S2 shows the saturation and cooling time constants according to differences in tile spacing and the modeled temperature distribution. The thermal time constant is determined by the amount of time it takes for the device to reach 63.2% of the maximum thermoelectric voltage observed because thermal time is defined as the time until the system's response decays to $1 - \frac{1}{e}$ (=63.2%) of that of the initial state (Figure S2a,b). While heating the thin PDMS layer placed between the thermoelectrics (L = 0.5 mm), thermal energy propagates stably throughout the entire device. However, for a device with a thick PDMS layer (L = 4.5 mm), significantly lower thermal conductivity of PDMS than that of Bi_2Te_3 impedes thermal propagation, resulting in delayed thermal saturation (Figure S2c). Consequently, the amount of time it takes for thermal saturation increases monotonically with increasing PDMS layer thickness. A similar trend is observed during cooling (Figure S2d). While the device with a 0.5 mm thick PDMS layer exhibits a characteristic cooling time of 0.59 s, the device with a 4.5 mm thick PDMS layer takes twice as long to reach 63.2% of cooling (1.74 s). It is noted that the characteristic time constants are much smaller for cooling than those for heating because cooling occurs in all directions as opposed to heating induced from a single surface and direction.

However, varied thermal insulation by PDMS does not affect the maximum instantaneous power generated from thermoelectrics. With PDMS widths varying from 0.5 to 4.5 mm, the instantaneous open circuit voltage (OCV) and short circuit current (SCC) remain the same at around 21.32 mV and 1.15 mA, respectively (Figure S3a). This is due to the fixed end-point temperatures used in this study, i.e., 35 °C for human skin and 20 °C for the ambient environment. Change in the hot-side temperature significantly affects the maximum instantaneous power (Figure S3b) and the Seebeck coefficients (Figure S3c). The electrical characteristics including matched impedance remain more or less unchanged with varied tile spacing (Figure S4). Because the end-point temperatures remain fixed for human touch-based energy harvesters, engineering the insulation provides a route to tune the temporal behavior of the generated power and thus maximize the time-averaged power output.

The triboelectric energy output highly depends on the input frequency, featuring much sharper voltage and current peaks

DOI: 10.1021/acsenergylett.9b01426
ACS Energy Lett. 2019, 4, 2069−2074

(Figure 2d and Figure S5a,b). At 1 Hz, the OCV and SCC peaks reach 10.5 V and 0.14 μA, respectively, for 2 mm of tile spacing. The peak output voltage increases monotonically with increasing input frequency for all tile spacings (Figure 2e), as reported in the literature.[19] This contrasts with thermoelectric generators where only the two end-point temperatures affect the peak output voltage. In addition, increased mechanical input results in escalated time-averaged triboelectric power (Figure S6). Hence, triboelectric energy output increases in terms of both peak power and average power, clearly demonstrating that triboelectric power output is best suited at harvesting high-frequency motion, i.e., above 10 Hz.

Interestingly, a decreasing trend in peak current width with respect to tile spacing is observed; the full width at half-maximum for the SCC peaks decreases from 125.3 to 107.5 ms as the tile spacing increases from 0.5 to 4.0 mm (Figure S5c). This critically affects the total triboelectric charge generated. For the same increase in tile spacing, the total charge increases by 20% from 0.0152 to 0.0182 μC (Figure S5d), while the volume of PDMS increases by 1177% (Table S1). Similarly, the volumetric power density decreases from 2.69 to 0.645 μW/cm^3 (Figure 2f). Such variations in power density and total charge generated sharply contrast with the conventional notion that the amount of generated triboelectric energy scales with the amount of active surface or volume of the triboelectric generator. Instead, small feature sizes result in efficient triboelectric energy harvesters.

Size-dependent triboelectric current duration calls for further understanding of its mechanism and design rules involving feature sizes. We note that the decreasing peak width according to the increasing tile spacing clearly rules out charge transport across the PDMS layer from the possible causes of the size-dependent triboelectric current generation. Rather, the interfacing Bi_2Te_3 tiles with high dielectric properties may affect the current duration. It has been recently reported that triboelectric generators with interfacing dielectric[20] or ionic gels[21] generate triboelectric current with increased peak widths. The complex charge-transfer mechanism at the interface between the PDMS and Bi_2Te_3 may reduce the decaying of generated charge, although the exact mechanism remains to be elucidated.

Component energy harvesters employed in the hybrid device exhibit distinct behavior according to the mechanical input frequency and feature sizes, thereby suggesting optimization strategies and design guidelines for the hybrid energy harvester. As the input frequency increases from 0.5 to 2.5 Hz, thermoelectric power generation saturates in terms of both peak power and time-averaged power (Figures 3a and S7a). The peak power slightly decreases owing to the insufficient heat transfer for power generation at frequencies above 1 Hz, and thermoelectric operation at high frequencies is expected to lower the output power via heat saturation. Hence, the optimal operational frequency for thermoelectrics lies around 2 Hz, although this can be tuned by engineering heat transport properties. For triboelectrics, the optimal operational frequency lies well above 5 Hz given the current duration is of approximately 120 ms (Figures3b and S7b).

Power density with respect to total device volume demonstrates the effect of feature size at 2.5 Hz (Figure 3c). As mentioned in Table S1, the increase in tile spacing indicates significantly increased volume fraction of triboelectric generators. The triboelectric power, however, remains almost identical despite the increase in PDMS volume, reflecting the strong feature-size effect. The thermoelectric power is inversely proportional to the tile spacing due to the decreased volume fraction. This clearly differs from the negligible effect of Bi_2Te_3 and PDMS thicknesses on power output (Figure S8) and demonstrates that increasing the PDMS−thermoelectric interface area per unit volume maximizes the total power density.

In an attempt to explore the variable space of input frequency and tile spacing, we estimate time-averaged power output for each component and the hybrid energy harvester according to time t and tile spacing L. The thermoelectric voltage output across the matched impedance of 16.8 Ω is fitted using the following exponential functions:

Mount region:

$$V_{\mathrm{mnt}}(t,L) = \mathrm{e}^{-0.18t+\ln 13.10} - \mathrm{e}^{(3.33\mathrm{e}^{-1461L}-2.56)t+\ln 13.01} \quad (1)$$

Saturation region:

$$V_{\mathrm{sat.}}(t,L) = \mathrm{e}^{(24.13L-0.22)t+\ln 6.69} + 3.08 \quad (2)$$

Cooling region:

$$V_{\mathrm{cool.}}(t,L) = \mathrm{e}^{-(1.52\mathrm{e}^{-774.1L}+0.34)t+\ln 10.34} - 0.58 \quad (3)$$

On the basis of these equations, the power output values for thermoelectric generators with tile spacing between 0.5 and 4.5 mm for targeted frequencies between 0.5 and 2.5 Hz are modeled (Figure S9−17). With the fitted voltage curves, the time-averaged power densities at different frequencies are estimated for the thermoelectric (Figure 3d), triboelectric (Figure 3e), and hybrid device with respect to the total device volume (Figure 3f).

The overall power density increases with increasing frequency and decreases with increasing tile spacing. For thermoelectrics, time-averaged power output increases with increasing input frequency because cooling-induced power loss occurs at low frequencies. The increasing power trend with respect to decreasing tile spacing (and thus increasing fill factor) clearly contrasts with recent reports on reducing the thermoelectric fill factor to maintain sufficient thermal gradients.[12] When operated with repeated touch and release, thermoelectrics do not require strict thermal insulation to prevent thermal saturation, thereby resulting in enhanced thermal power with an increased fill factor. In terms of power density, this fill factor-induced power output clearly exceeds the effect of power output from thermal insulation thickness formed using PDMS (Figure S7a). Time-averaged triboelectric power density remains almost unchanged with respect to tile spacing due to the strong feature-size effect; however, it increases sharply with increasing frequency. Optimized power output occurs at 2.5 Hz of frequency and 0.5 mm of tile spacing, resulting in 3.27 μW/cm^3 of output power density. This power density is comparable to the average power consumption of a Bluetooth LE device.

In addition, it has recently been reported that the triboelectrification upon contact follows the thermionic emission model and thus, hotter solids tend to get positively charged.[22] This leads to the design guideline for HThTG that the cold side must be negative-charging materials and the hot side be positive-charging materials. In our device, we harvest the thermal energy from human skin, the positive-charging material, to the cold side of PDMS, the negative-charging material.

The optimization process demonstrated in this work provides several general implications for improving HThTGs. First, the

DOI: 10.1021/acsenergylett.9b01426
ACS Energy Lett. 2019, 4, 2069−2074

optimal operating frequency of a hybrid energy harvester can be defined to be the threshold frequency under which its thermal saturation occurs. The optimized frequency also implies that an energy harvester can be designed to harvest specifically targeted frequency human motion. This optimal frequency is mainly determined by the heat transport properties provided by the interfacing triboelectric materials. Second, triboelectric power density can be maximized by increasing the interface area between triboelectric materials and high-dielectric thermoelectrics. Although the exact mechanism by which the interface boosts the triboelectric charges remains to be elucidated, we demonstrated in this work that decreasing the thickness of the PDMS layer down to 5 mm significantly increases the volumetric power density. Designing a device using small Bi_2Te_3 tiles with thin spacings filled with PDMS is expected to increase the power output significantly.

In summary, we present an HThTG capable of achieving a time-averaged power density of 3.27 $\mu W/cm^3$ when operated by human touch at a frequency of 2.5 Hz. Optimizing the hybrid generator in terms of operating frequency and feature size establishes the design guidelines of maximizing thermoelectric−triboelectric interface area and preventing thermal saturation. An interesting feature-size-dependent triboelectric charge generation and a high fill factor benefiting thermoelectric power generation techniques are revealed. The resultant hybrid generator outperforms the simple addition of each component of an energy harvester and demonstrates that energy harvesting in human time scales (0.5−2.5 Hz) can also generate technologically relevant microwatts of average power with potential application in various human touch environments such as doorknobs, guardrails, and keyboards.

■ ASSOCIATED CONTENT

Supporting Information

The Supporting Information is available free of charge on the ACS Publications website at DOI: 10.1021/acsenergylett.9b01426.

> Experimental section including detailed characterization of material properties and measurement methods, table of PDMS surface area and volume according to tile spacing, and figures showing the fabrication process of HThTG, modeled heat transport phenomena within the HThTG and comparison with the experimental results, electrical characteristics of the thermoelectric part of the HThTG, impedance matching of the thermoelectric part of the HThTG, SCC data, triboelectric voltage and power obtained at varied mechanical input load, power densities of thermoelectric and triboelectric generators, peak current outputs, output voltage signals for the HThTG with respect to varying tile spacing, and images of the apparatus for triboelectric performance evaluation (PDF)

■ AUTHOR INFORMATION

Corresponding Authors

*S.K. E-mail: stkim@kist.re.kr.

*W.C. E-mail: wojchoi@korea.ac.kr.

ORCID

Sangtae Kim: 0000-0002-7959-8249

Wonjoon Choi: 0000-0002-1913-598X

Author Contributions

[§]These authors contributed equally to this work.

Notes

The authors declare no competing financial interest.

■ ACKNOWLEDGMENTS

This work was supported by the Ministry of Trade, Industry & Energy (MOTIE, Korea) under the Industrial Technology Innovation Program (10080611), the Korea Institute of Energy Technology Evaluation and Planning (KETEP), and the Ministry of Trade, Industry & Energy (MOTIE) of the Republic of Korea (Grant no. 20173010032170). S.K. acknowledges the support from the National Research Council of Science & Technology (NST) grant by the Korea government (MSIP) (No. CAP-17-04-KRISS) and the Korea Institute of Science and Technology (KIST) (No. 2E29400 and 2E28990).

■ REFERENCES

(1) Fan, F. R.; Tang, W.; Wang, Z. L. Flexible nanogenerators for energy harvesting and self-powered electronics. *Adv. Mater.* **2016**, *28* (22), 4283−4305.

(2) Seo, B.; Hwang, H.; Kang, S.; Cha, Y.; Choi, W. Flexible-detachable dual-output sensors of fluid temperature and dynamics based on structural design of thermoelectric materials. *Nano Energy* **2018**, *50*, 733−743.

(3) Riffat, S. B.; Ma, X. Thermoelectrics: a review of present and potential applications. *Appl. Therm. Eng.* **2003**, *23* (8), 913−935.

(4) Gao, C.; Lee, S. W.; Yang, Y. Thermally regenerative electrochemical cycle for low-grade heat harvesting. *ACS Energy Letters* **2017**, *2* (10), 2326−2334.

(5) Bhatia, D.; Kim, W.; Lee, S.; Kim, S. W.; Choi, D. Tandem triboelectric nanogenerators for optimally scavenging mechanical energy with broadband vibration frequencies. *Nano Energy* **2017**, *33*, 515−521.

(6) Chen, F.; Wu, Y.; Ding, Z.; Xia, X.; Li, S.; Zheng, H.; Diao, C.; Yue, G.; Zi, Y. A novel triboelectric nanogenerator based on electrospun polyvinylidene fluoride nanofibers for effective acoustic energy harvesting and self-powered multifunctional sensing. *Nano Energy* **2019**, *56*, 241−251.

(7) Muralidharan, N.; Li, M.; Carter, R. E.; Galioto, N.; Pint, C. L. Ultralow Frequency Electrochemical−Mechanical Strain Energy Harvester Using 2D Black Phosphorus Nanosheets. *ACS Energy Letters* **2017**, *2* (8), 1797−1803.

(8) Kim, S.; Choi, S. J.; Zhao, K.; Yang, H.; Gobbi, G.; Zhang, S.; Li, J. Electrochemically driven mechanical energy harvesting. *Nat. Commun.* **2016**, *7*, 10146.

(9) Wang, S.; Lin, L.; Wang, Z. L. Triboelectric nanogenerators as self-powered active sensors. *Nano Energy* **2015**, *11*, 436−462.

(10) Hwang, H.; Lee, K. Y.; Shin, D.; Shin, J.; Kim, S.; Choi, W. Metal-free, flexible triboelectric generator based on MWCNT mesh film and PDMS layers. *Appl. Surf. Sci.* **2018**, *442*, 693−699.

(11) Zhao, L.-D.; Lo, S.-H.; Zhang, Y.; Sun, H.; Tan, G.; Uher, C.; Wolverton, C.; Dravid, V. P.; Kanatzidis, M. G. Ultralow thermal conductivity and high thermoelectric figure of merit in SnSe crystals. *Nature* **2014**, *508* (7496), 373.

(12) Lee, Y. G.; Kim, J.; Kang, M. S.; Baek, S. H.; Kim, S. K.; Lee, S. M.; Lee, J.; Hyun, D. B.; Ju, B. K.; Moon, S. E. Design and experimental investigation of thermoelectric generators for wearable applications. *Adv. Mater. Technol.* **2017**, *2* (7), 1600292.

(13) Chun, J.; Ye, B. U.; Lee, J. W.; Choi, D.; Kang, C.-Y.; Kim, S.-W.; Wang, Z. L.; Baik, J. M. Boosted output performance of triboelectric nanogenerator via electric double layer effect. *Nat. Commun.* **2016**, *7*, 12985.

(14) Hwang, G. T.; Park, H.; Lee, J. H.; Oh, S.; Park, K. I.; Byun, M.; Park, H.; Ahn, G.; Jeong, C. K.; No, K. Self-powered cardiac pacemaker enabled by flexible single crystalline PMN-PT piezoelectric energy harvester. *Adv. Mater.* **2014**, *26* (28), 4880−4887.

(15) Ryu, H.; Yoon, H. J.; Kim, S. W. Hybrid Energy Harvesters: Toward Sustainable Energy Harvesting. *Adv. Mater.* **2019**, 1802898.

DOI: 10.1021/acsenergylett.9b01426
ACS Energy Lett. 2019, 4, 2069−2074

(16) Lee, S.; Bae, S.-H.; Lin, L.; Ahn, S.; Park, C.; Kim, S.-W.; Cha, S. N.; Park, Y. J.; Wang, Z. L. Flexible hybrid cell for simultaneously harvesting thermal and mechanical energies. *Nano Energy* **2013**, *2* (5), 817−825.

(17) Wang, X.; Wang, Z. L.; Yang, Y. Hybridized nanogenerator for simultaneously scavenging mechanical and thermal energies by electromagnetic-triboelectric-thermoelectric effects. *Nano Energy* **2016**, *26*, 164−171.

(18) Suo, G.; Yu, Y.; Zhang, Z.; Wang, S.; Zhao, P.; Li, J.; Wang, X. Piezoelectric and triboelectric dual effects in mechanical-energy harvesting using BaTiO3/polydimethylsiloxane composite film. *ACS Appl. Mater. Interfaces* **2016**, *8* (50), 34335−34341.

(19) Jirayupat, C.; Wongwiriyapan, W.; Kasamechonchung, P.; Wutikhun, T.; Tantisantisom, K.; Rayanasukha, Y.; Jiemsakul, T.; Tansarawiput, C.; Liangruksa, M.; Khanchaitit, P. Piezoelectric-induced triboelectric hybrid nanogenerators based on the ZnO nanowire layer decorated on the Au/polydimethylsiloxane−Al structure for enhanced triboelectric performance. *ACS Appl. Mater. Interfaces* **2018**, *10* (7), 6433−6440.

(20) Chen, J.; Guo, H.; He, X.; Liu, G.; Xi, Y.; Shi, H.; Hu, C. Enhancing performance of triboelectric nanogenerator by filling high dielectric nanoparticles into sponge PDMS film. *ACS Appl. Mater. Interfaces* **2016**, *8* (1), 736−744.

(21) Ye, B. U.; Kim, B.-J.; Ryu, J.; Lee, J. Y.; Baik, J. M.; Hong, K. Electrospun ion gel nanofibers for flexible triboelectric nanogenerator: electrochemical effect on output power. *Nanoscale* **2015**, *7* (39), 16189−16194.

(22) Lin, S.; Xu, L.; Xu, C.; Chen, X.; Wang, A. C.; Zhang, B.; Lin, P.; Yang, Y.; Zhao, H.; Wang, Z. L. Electron Transfer in Nanoscale Contact Electrification: Effect of Temperature in the Metal−Dielectric Case. *Adv. Mater.* **2019**, *31*, 1808197.

DOI: 10.1021/acsenergylett.9b01426
ACS Energy Lett. 2019, 4, 2069−2074